



Apparent diffusion coefficient (ADC): A potential in vivo biological surrogate of the incidentally discovered bone lesions at 3T MRI

M.R. Nohu^{a,*}, Ahmed Doweidar^b, Abdullah Mohie-Eddin Khalil^c

^a Department of Radiology, Faculty of Medicine, Alexandria University, Egypt

^b Department of Radiology, SWBH NHS TRUST, Birmingham, West Midlands B187QH, UK

^c Department of Radiology and Clinical Imaging, El-Razi Hospital, Gamal Abd El-Nasser Street, Sulibakhat, 13001 Kuwait City, Kuwait

HIGHLIGHTS

- ADC is a diffusion metric that could address tissue micro-environment noninvasively.
- ADC is a non-invasive, in-vivo surrogate that is capable to discern osseous lesions into benign or malignant.
- In proper clinical situations, this might mitigate the need for use of contrast and further diagnostic workup.

ARTICLE INFO

Keywords:

Bone lesions
Diffusion-weighted (DW)
Apparent diffusion co-efficient (ADC) magnetic
resonance imaging (MRI)
3 Tesla (3T)

ABSTRACT

Purpose: To probe the potential of apparent diffusion coefficient (ADC) to rectify the incidentally detected bone lesion on MRI into benign or malignant lesions.

Materials and methods: We retrospectively recruited 44 patients (24 males and 20 females); with 52 bone lesions, who underwent diffusion weighted (DW) imaging using multiple b-values on 3 T MRI. ADC maps were derived and analyzed by two radiologists; blinded to the final diagnosis. The mean ADC values were used for statistical analyses. The diagnosis was deduced by histopathological confirmation; in 32 lesions and strict clinical and imaging follow-up for at least 12 months; in 20 lesions.

Results: The mean ADC value (mean±SD) of all malignant tumors (including cartilaginous neoplasms) was $[0.92 \pm 0.40] \times 10^{-3} \text{ mm}^2/\text{s}$. This significantly differed from those of both primary benign tumors $[1.14 \pm 0.24] \times 10^{-3} \text{ mm}^2/\text{s}$, ($p = 0.011$), and all non-malignant lesions collectively $[1.29 \pm 0.44] \times 10^{-3} \text{ mm}^2/\text{s}$, ($p < 0.001$). Using mADC value of $\leq 1.1 \times 10^{-3} \text{ mm}^2/\text{s}$ resulted in 86.1% sensitivity and 62.5% specificity for characterizing a lesion as a malignant. The inter-rater reliability was almost perfect (95% CI = 0.954–0.985).

Conclusion: ADC could be a non-invasive in-vivo surrogate that may be able to discern the incidentally discovered osseous lesions into benign and malignant pathologies and guide further diagnostic workup.

1. Introduction

The incidental detection of a skeletal lesion of indeterminate imaging features may instigate a myriad of further advanced imaging and even the more invasive bone biopsy procedures [1].

The role of MR in evaluation of various skeletal lesion is well established thanks to its exquisite anatomical details, multiplanar capabilities and lack of radiation [2]. A recent meta-analysis confirmed its superiority to other imaging methods in characterizing bony lesions [3].

Recently, growing concerns about radiation hazards and latent accumulations of gadolinium-based agents in different body tissues, initiated more interest in safer alternative diagnostic utilities [4,5]. Therefore, there is a growing interest in clinically feasible non-invasive biomarkers that might have the potentials to discern the biological dignity of incidentally encountered bone lesions into innocent and sinister entities with subsequent different patient's management planes.

Diffusion weighted imaging (DWI) is a functional MR sequence that is capable of non-invasive probing of tissues' microenvironment by

* Correspondence to: Faculty of Medicine, Alexandria University, Egypt.

E-mail addresses: mragab73@yahoo.com, mohamed.nouh@alexmed.edu.eg (M.R. Nohu), ahmeddoweidar1@yahoo.com (A. Doweidar), Abdullah.m.khalil@gmail.com (A.M.-E. Khalil).

¹ Current address: Department of Radiology, Armed Force Hospital, King Abd El-Aziz Airbase, Dhahran 31932, Saudi Arabia.

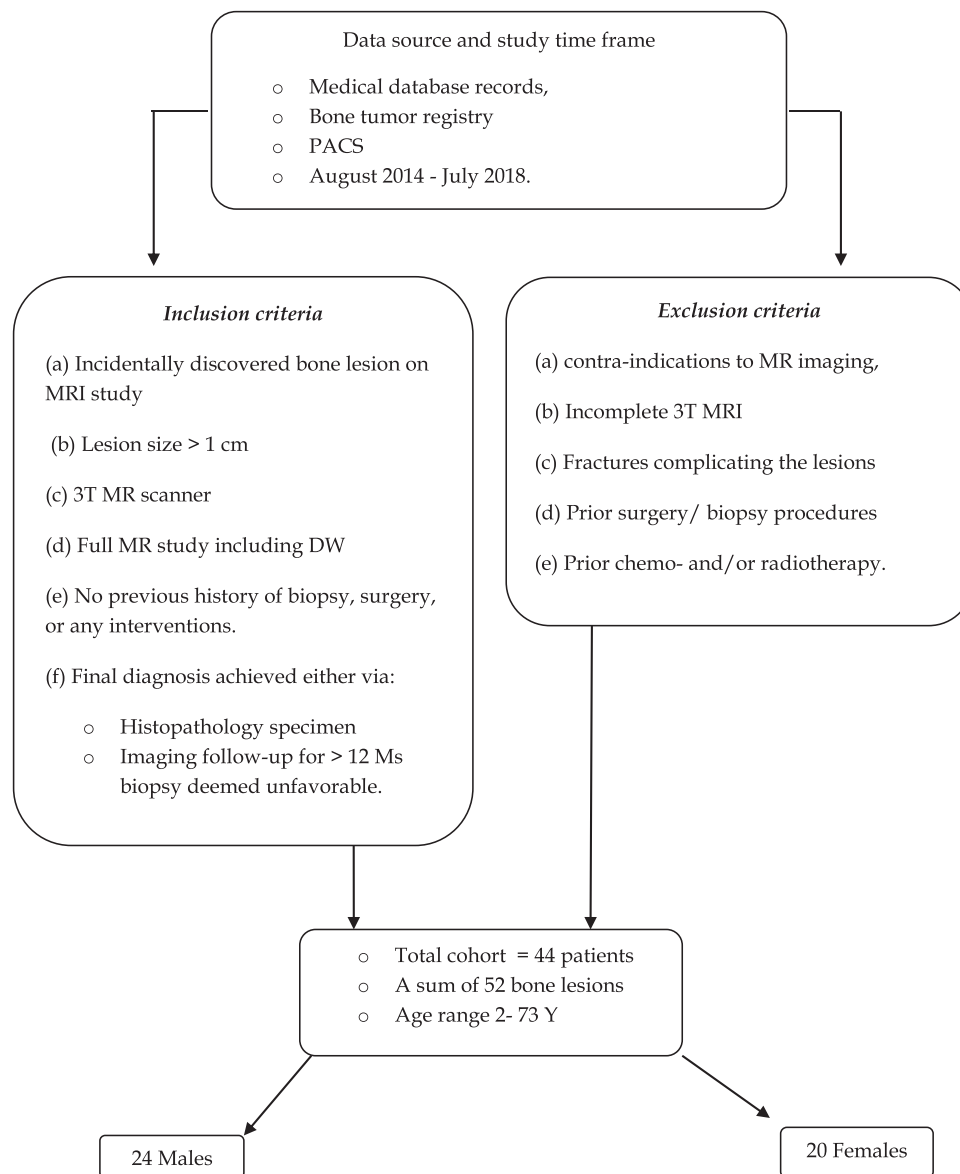


Fig. 1. Flow diagram of study cohort selection.

addressing the microscopic motion of its water molecules and reflecting its cellularity, from both qualitative and quantitative perspectives [6]. Consequently, growing interest in clinical utility of DW in differentiating skeletal benign and malignant lesions has increased yet the results of available research are somewhat variable and even controversial [7–10].

In this sense, DW could be a one-stop shop non-invasive imaging tool, which can be used to probe tissue dignity in vivo. As such, we sought to probe the potential of apparent diffusion coefficient (ADC) in rectifying incidental bone lesions into benign or malignant tumors on magnetic resonance imaging (MRI).

2. Materials and methods

2.1. Study design and research ethics

This study was approved by our local institutional review board with patients' consent waiver due to the retrospective study design.

2.2. Study population

Our study cohort has been extracted from our hospital's medical database records, bone tumor registry and PACS (picture archiving and communication system) over the period of 1st August 2014–31 July 2018 according to certain inclusive and exclusive criteria illustrated in Fig. 1 for simple clarification.

Incidentally discovered bone lesion on MRI study was defined as a lesion that first reported on the current MR study, or a new lesion when compared to an available prior MR study of the same patient. We did not include sub-centimeter lesions to rule out potential readout errors on DW. Furthermore, we only included comprehensive conventional MR study on our 3 T scanner with DW images of adequate diagnostic quality, evaluated by one of the authors. Thus, a total of 44 patients; with a sum of 52 bony lesions, who matched our designated inclusion and exclusion criteria had been recruited to form our current study cohort.

2.3. Routine MR imaging

All MRI scans were conducted using a 3-T scanner (GE Discovery MR 750w) equipped with high-definition multichannel body and/or local

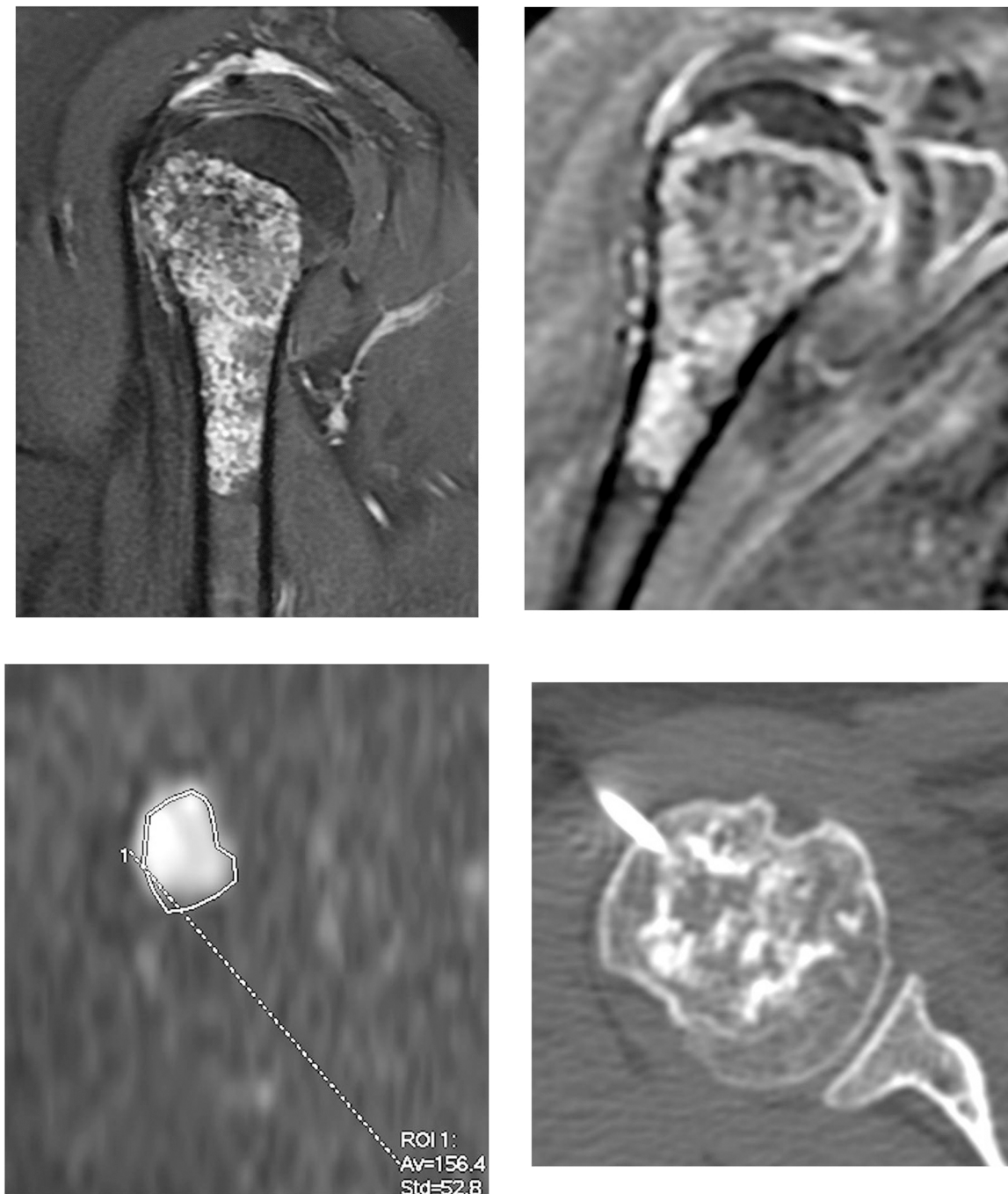


Fig. 2. A 58 Y female with shoulder pain. (a) Sagittal PD FS and (b) Post-GAD images show replacement of the bone marrow of the proximal humerus with a predominantly high signal lesion with wide zone of transition. The lesion has a large solid portion along the posterior humeral cortex of the proximal shaft. It exhibits low signal intensity on PD FS (a) with corresponding notable contrast enhancement on (b). (c) Axial ADC map of the lesion showing placement of the ROI around this part to measure mADC. (d) CT guided biopsy of the lesion proved to be Chondrosarcoma G-II on histopathology.

array coils suitable for the examined body part for best imaging quality. Pre-contrast conventional MRI images were obtained in the orthogonal anatomical planes that depict well the examined lesion and its extents. It included T1-weighted for the exquisite anatomic details and fat suppressed (FS) T2-and/or PD weighted to highlight pathology depiction. The slice thickness, field of view (FOV) and image matrix were variable according to the examined body region to ensure adequate coverage of the studied anatomic region, depiction of the lesion and high-quality images satisfactory for clinical diagnosis.

Moreover, our routine post-contrast MR images included enhanced T1-weighted images performed in the three orthogonal planes using the corresponding pre-contrast imaging parameters.

2.4. Diffusion-weighted (DW) MR imaging

Our institute's protocol is to obtain all DW images prior to contrast administration. Following field homogenization, using inversion recovery pulse sequence (TI=180 ms) to mitigate chemical shift artifacts, a single-shot echo-planar imaging (SS-EPI) pulse sequence is deployed to acquire the DW images using parallel imaging and array coil spatial sensitivity encoding (ASSET) techniques. The following parameters were used: TR/TE effective range, 3500 to 6200/70–100 ms; slice thickness/intersection gap, 5/0.5 mm; matrix, 128 × 128; and suitable field of view (FOV) to adequately cover the examined anatomical region. Three b-values of: 0, 500 and 1000 s/mm² were applied in three

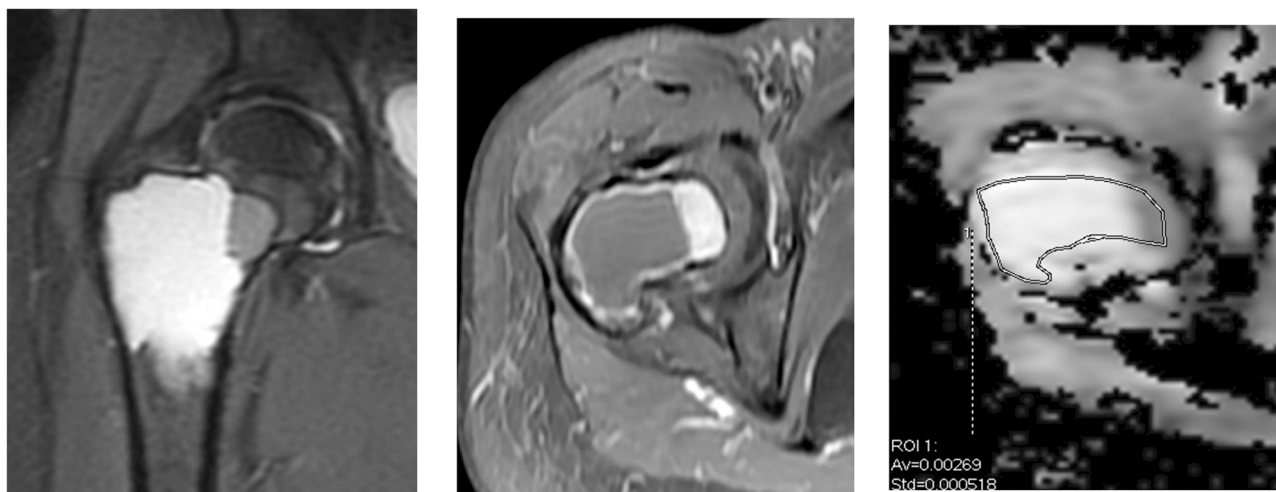


Fig. 3. A 18 Y male presented with right hip pain. (a) Coronal PD FS and (b) Axial post-GAD images show a simple bone cyst replacing the bone marrow of the proximal femoral diaphysis with narrow zone of transition and no enhancement. (c) Axial ADC image showing the global inclusion of the lesion to measure the mADC.

Table 1
The skeletal topographic distribution of the studied bony lesions.

Skeleton	Anatomical part	Lesion's number (%)
Appendicular	Clavicle	1 (1.9)
	Humerus	4 (7.7)
	Ulna	1 (1.9)
	Radius	1 (1.9)
	Phalanx	1 (1.9)
	Femur	16 (30.8)
	Tibia	5 (9.6)
Axial	Skull base	1 (1.9)
	Spine- cervical	2 (3.8)
	Spine- dorsal	4 (7.7)
	Spine- lumbar	2 (3.8)
	Spine-sacrum	2 (3.8)
	Pelvis- iliac bone	8 (15.4)
	Pelvis- ischial bone	2 (3.8)
	Pelvis- pubic bone	2 (3.8)
	Total	52 (100)

orthogonal anatomical planes with three averages used to improve signal to noise ratio (SNR) due to the inherently low SNR of the bone marrow. The DW images acquisition time was in the range of 3–4 min. Pixel-based apparent diffusion coefficient (ADC) images and maps were generated using all used 3 b-values via pre-defined mathematic algorithms (Functool software specific for DWI analysis), for optimal assessment of the bone marrow, on the accompanying Advantage Workstation 4.6 (GE Healthcare, USA) and archived in each patient's image files.

2.5. Image analysis

MR images were pushed to our PACS and images were analyzed independently by two musculoskeletal radiologists of 15 and 10 years of experience in musculoskeletal imaging, respectively. Initially, each reader analyzed the conventional pre- and post-contrast imaging findings for the topography of the lesion, its signal criteria and pattern of enhancement following intravenous gadolinium administration. Afterwards, DW and ADC images were interpreted.

On DW images, the ADC readout was sampled using axial images. We manually fitted our region of interest (ROI) to the most solid part of the lesion. This was **defined as the region that fulfills: (a)** high/intermediate signal intensity on T2-W images and DWI of $b=0 \text{ s/mm}^2$, **(b)** low T1- signal intensity and **(c)** enhanced on post-contrast T1-weighted

images, on the concurrent conventional studies. We used the mean ADC value similar to previous models in both axial and appendicular skeletons [9,10].

Cross-reference to the conventional MR images was practised to exclude necrotic, hemorrhagic and calcific foci that may affect readouts. In lesions containing multiple solid areas, only the biggest portion of the tumor was encompassed and sampled to be expressive of the whole lesion (Fig. 2). Alternatively, predominantly cystic bone lesions were globally encompassed in the ROI owing to their suggested nature on conventional MR images (Fig. 3).

Likewise, cross-matched ROIs were copied and used to sample adjacent normal bone marrow in reference to conventional T1W and fat-suppressed water-sensitive images and the (mADC) values were recorded as a reference value.

2.6. Reference standard

Histopathological diagnosis has been secured in thirty-two lesions in our study group either via imaging guided biopsy and/or surgical specimens. The biopsied lesions were chosen following the general bone biopsy guidelines and previously published reproducible methodology [11,12]. The remaining twenty lesions were diagnosed by their established specified imaging criteria as well as clinical and imaging follow-up for at least 12 months.¹

2.7. Statistical analysis

Data were coded and entered using the statistical package SPSS (Statistical Package for the Social Sciences) IBM SPSS® statistics version 2.2 (IBM® Corp., Armonk, NY, USA). Qualitative data were expressed as frequency and percentage; and were tested using Pearson's Chi-square test. Numerical data were expressed as mean and standard deviation or median and range as appropriate. Comparisons between quantitative variables were done using the non-parametric Mann-Whitney test.

Receiver operating Characteristic (ROC) curve was constructed with area under curve analysis performed to detect the best cut-off value of ADC for detection of malignancy. The inter-rater reliability was tested

¹ Kindly be informed that reference 12 is: M.R. Nough, H.M. Abu Shady, Initial CT-guided needle biopsy of extremity skeletal lesions: Diagnostic performance and experience of a tertiary musculoskeletal center, Eur. J. Radiol. 83 (2014) 360–365. <https://doi.org/10.1016/j.ejrad.2013.10.012>.

Table 2
Comparison of ADC values of the included 52 bone lesions.

Lesion	Age	Gender	Diagnosis	Location	Pathological Group	Mean ADC \pm SD ($\times 10^{-3}$ mm ² /s)
1	11	F	Ewing's sarcoma	Tibia	1ry malignant	0.79 \pm 0.10
2	7	F	Ewing's sarcoma	Femur	1ry malignant	0.74 \pm 0.14
3	41	M	Ewing's sarcoma	Femur	1ry malignant	0.41 \pm 0.11
4	28	M	Ewing's sarcoma	Femur	1ry malignant	0.53 \pm 0.13
5	15	M	Ewing's sarcoma	Ilium	1ry malignant	1.03 \pm 0.16
6	47	M	Primary lymphoma	Femur	1ry malignant	0.86 \pm 0.18
7	37	M	Primary lymphoma	Femur	1ry malignant	0.81 \pm 0.05
8	58	F	Chondrosarcoma	Humerus	1ry malignant	2.08 \pm 0.30
9	43	M	Chondrosarcoma	Clavicle	1ry malignant	1.85 \pm 0.25
10	40	F	Chondrosarcoma	Humerus	1ry malignant	2.16 \pm 0.32
11	20	F	Osteosarcoma	Femur	1ry malignant	0.65 \pm 0.18
12	44	M	Osteosarcoma	Tibia	1ry malignant	1.14 \pm 0.30
13	24	M	Osteosarcoma	Tibia	1ry malignant	0.64 \pm 0.17
14	32	M	Osteosarcoma	Femur	1ry malignant	1.01 \pm 0.12
15	50	M	Multiple myeloma	Humerus	1ry malignant	1.08 \pm 0.14
16	31	F	Plasmacytoma	Femur	1ry malignant	0.74 \pm 0.23
17	48	F	Breast adenoca. metastasis	C. spine	2ry malignant	0.82 \pm 0.23
18	48	F	Breast adenoca. metastasis	Skull base	2ry malignant	0.92 \pm 0.39
19	56	F	Breast adenoca. metastasis	Pubis	2ry malignant	0.98 \pm 0.12
20	56	F	Breast adenoca. metastasis	C. spine	2ry malignant	0.66 \pm 0.27
21	68	F	Breast adenoca. metastasis	Sacrum	2ry malignant	0.94 \pm 0.14
22	68	F	Breast adenoca. metastasis	Femur	2ry malignant	1.05 \pm 0.16
23	58	F	Breast adenoca. metastasis	Femur	2ry malignant	1.25 \pm 0.12
24	41	F	Breast adenoca. metastasis	T. spine	2ry malignant	1.09 \pm 0.11
25	69	F	Breast adenoca. metastasis	Femur	2ry malignant	0.77 \pm 0.16
26	59	F	Breast adenoca. metastasis	Ilium	2ry malignant	0.73 \pm 0.14
27	40	F	Breast adenoca. metastasis	Acetabulum	2ry malignant	0.97 \pm 0.20
28	40	F	Breast adenoca. metastasis	Sacrum	2ry malignant	1.08 \pm 0.09
29	64	F	Breast adenoca. metastasis	Femur	2ry malignant	0.86 \pm 0.15
30	65	F	Cervix adenoca. metastasis	T. spine	2ry malignant	1.09 \pm 0.20
31	68	M	Prostate adenoca. metastasis	Acetabulum	2ry malignant	0.46 \pm 0.07
32	68	M	Prostate adenoca. metastasis	Ischium	2ry malignant	0.49 \pm 0.07
33	73	M	Prostate adenoca. metastasis	Acetabulum	2ry malignant	0.58 \pm 0.14
34	73	M	Prostate adenoca. metastasis	Ilium	2ry malignant	0.65 \pm 0.16
35	72	M	Prostate adenoca. metastasis	Ilium	2ry malignant	0.76 \pm 0.09
36	68	M	Prostate adenoca. metastasis	Ischium	2ry malignant	0.71 \pm 0.12
37	26	M	GCT	Phalanx	1ry benign	1.11 \pm 0.19
38	24	M	GCT	Tibia	1ry benign	1.00 \pm 0.16
39	46	M	GCT	Femur	1ry benign	0.99 \pm 0.12
40	44	F	GCT	L. spine	1ry benign	1.22 \pm 0.12
41	30	M	GCT	Femur	1ry benign	1.00 \pm 0.14
42	29	F	GCT	Radius	1ry benign	0.91 \pm 0.02
43	22	F	GCT	Femur	1ry benign	0.87 \pm 0.11
44	44	F	Hemangioma	T. spine	1ry benign	1.35 \pm 0.10
45	41	F	Hemangioma	L. spine	1ry benign	1.28 \pm 0.12
46	38	M	Hemangioma (aggressive)	T. spine	1ry benign	1.67 \pm 0.18
47	2	M	Histiocytosis	Tibia	Tumor-like solid	1.04 \pm 0.17
48	16	M	Fibrous dysplasia	Pubis	Tumor-like solid	1.32 \pm 0.11
49	6	M	Fibrous dysplasia	Humerus	Tumor-like solid	1.29 \pm 0.31
50	17	M	ABC	Ilium	Tumor-like cystic	1.45 \pm 0.86
51	13	M	ABC	Ulna	Tumor-like cystic	1.49 \pm 0.68
52	36	F	SBC	Femur	Tumor-like cystic	2.69 \pm 0.52

by using the Intra Class Coefficient (ICC) and Cronbach's alpha reliability coefficient with their 95% confidence interval (95%CI). All tests were two-tailed and results were considered significant if p-value < 0.05.

3. Results

3.1. Study demographics and lesions' criteria

The study group included 44 patients (24 males and 20 females); ranging in age from 2 to 73 years (mean/median age, 39.2/40 years) with a total of 52 bone lesions, equally distributed in males and females (26 lesions in each gender). The skeletal topographic distribution of the studied bone lesions is shown in (Table 1). The most involved bones were the femur and iliac bones.

Although, the patients' sex was not a reliable discriminator between malignant and non-malignant lesions ($p = 0.229$), it has been noted that the malignant group was significantly ($p < 0.001$) older than non-

malignant group (the median age/range of malignant and non-malignant bone lesions was 48/7–73 and 27.5/2–46; respectively).

Eight of our patients had dual lesions (six patients had metastatic lesions, one patient had two benign lesions and the last one had a synchronous solitary metastatic and benign lesion). In contrast, the remaining thirty-six patients of our cohort had solitary lesions.

According to their pathologic biological behavior, the studied lesions have been dichotomized into malignant and benign lesions. Furthermore, the malignant lesions were categorized into primary 16/52 (30.8%) and secondary malignant 20/52 (38.5%) tumors. Alternatively, the non-malignant lesions were stratified as primary benign bone tumors 10/52 (19.2%), tumor-like solid 3/52 (5.8%) and tumor-like cystic bone lesions 3/52 (5.8%), (Table 2).

According to the final diagnostic methodology (Table 3), of the 32 (61.5%) lesions diagnosed by histopathological specimens, 25 lesions have been diagnosed via CT guided biopsy procedures that secured sufficient specimens to confidently conclude the final tissue diagnosis. These included: 16 primary malignant bone tumors, 7 giant cell tumors

Table 3
The distribution of diagnostic references of the studied lesions.

Method of diagnosis	Benign tumors (n = 10)	Malignant tumors (n = 36)	Benign tumor-like solid lesions (n = 3)	Benign tumor-like cystic lesions (n = 3)
Histopathologic confirmation (n = 32)	GCT (n = 7) Aggressive hemangioma (n = 1)	Chondrosarcoma (n = 3) Osteosarcoma (n = 4) Plasmacytoma (n = 1) Multiple Myeloma (n = 1) Ewing's sarcoma (n = 5) Primary Lymphoma (n = 2) Metastasis (n = 3)	Histiocytosis (n = 1) Fibrous dysplasia (n = 1)	SBC (n = 1) ABC (n = 2)
≥ 12 months of follow up confirming pre-settled clinical and imaging features (n = 20)	Hemangiomas (n = 2)	Metastasis (n = 17)	Fibrous dysplasia (n = 1)	

(GCTs), a single lesion of fibrous dysplasia, and an osseous histiocytic granuloma. The remaining 7 lesions; included: 3 bone cysts, 3 metastatic lesions and a case of an aggressive spinal hemangioma; had been diagnosed via open surgical biopsies as a part of their management.

On the other hand, 20 (38.5%) lesions; including 2 spine hemangiomas, a fibrous dysplasia and 17 metastatic lesions; were diagnosed by their specified imaging criteria as well as clinical and imaging follow-up for at least 12 months.

3.2. DW MR criteria

The mean ADC (mADC) value of the different categories of included bone lesions were calculated and compared (Table 2).

The mADC value of all malignant tumors (including cartilaginous neoplasms) was (mean±SD; [0.92 ± 0.40] ×10⁻³ mm²/s). This significantly differed from those of both primary benign tumors (mean±SD, [1.14 ± 0.24] ×10⁻³ mm²/s), (p = 0.011), and all non-malignant lesions collectively (including primary benign tumors, tumor-like solid and tumor-like cystic lesions) (mean±SD, [1.29 ± 0.44] ×10⁻³ mm²/s), (p < 0.001).

Paradoxically, the mean ADC value of the malignant chondroid lesions subgroup (mean±SD, [2.03 ± 0.16] ×10⁻³ mm²/s) was higher than that of the rest of malignant tumors (mean±SD, [0.82 ± 0.22] ×10⁻³ mm²/s), (median, 0.81 ×10⁻³ mm²/s) approaching to the readout of our case of simple bone cyst. Notably; after chondroid subgroup exclusion, the malignant tumors exhibited a more significant statistical difference from benign tumors (p = 0.001), and all non-malignant lesions (p < 0.001).

A receiver operating curve analysis (ROC) derived cut-off mean ADC value of ≤ 1.1 × 10⁻³ mm²/s resulted in a sensitivity and specificity of 86.1% and 62.5%; respectively for characterizing a lesion as a malignant. Moreover, an area under the curve of 0.813 validated it as a good tool to discern benign and malignant lesions (95% confidence interval (CI) 0.697–0.928; p < 0.001), (Fig. 4). When chondral lineage neoplasms have been excluded, the same mean ADC cut-off value resulted in a sensitivity of 93.9%, specificity of 62.5% and an area under ROC curve of 0.881 (95% confidence interval (CI) 0.786–0.976) (p < 0.001) for detecting malignancy, (Fig. 5). The inter-rater reliability was almost perfect (Cronbach's alpha = 0.987; ICC= 0.974, 95% CI = 0.954–0.985).

4. Discussion

Our current study investigated DW potentials to discern the incidental bone lesions into a benign process where follow-up may be the only action just needed or a sinister pathology that warrant further action without delay in patient management.

Demographically, the current study revealed higher prevalence of malignant bone lesions in older age groups, in contrast to benign bone lesions that prevail in younger age. Moreover, pelvic bones and femur hosted the highest number of lesions. This is in line with published previous literature [10,13]. We did not find significant sex difference

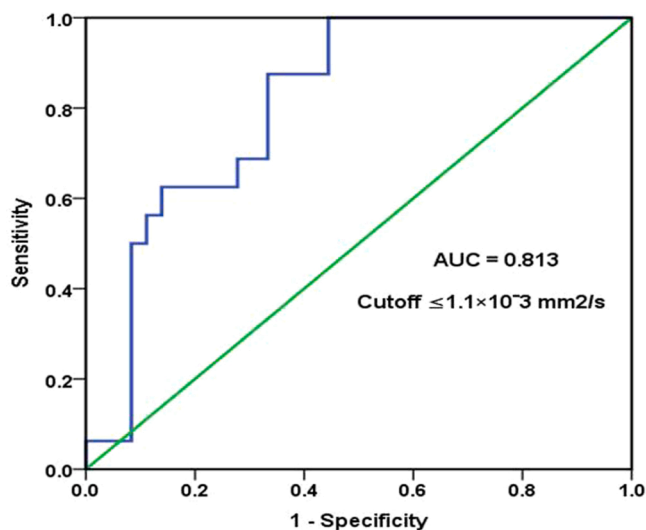


Fig. 4. Receiver operating curve (ROC) of mean ADC value for differentiating malignant from non-malignant bone lesions. Diagonal segments are produced by ties. The area under the ROC curve is 0.813(95% confidence interval: 0.697–0.928).

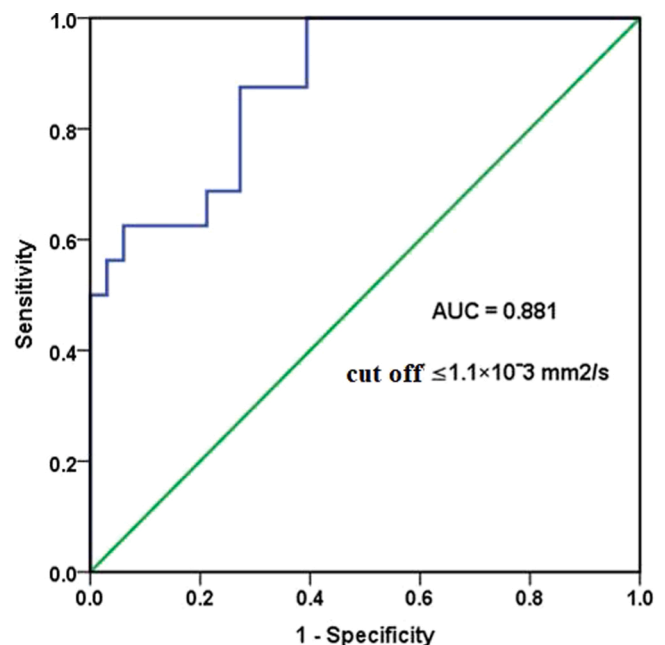


Fig. 5. Receiver operating curve (ROC) of mean ADC value for differentiating malignant from non-malignant bone lesions after exclusion of chondroid lesions. Diagonal segments are produced by ties. The area under the ROC curve is 0.881 (95% confidence interval: 0.786–0.976).

between either bone lesion groups.

Diffusion weighted is a functional MR tool that can address tissue cellularity and its microenvironment by monitoring water molecules motion. The (ADC) is an objective quantitative index of this peculiar tissue's water micro-molecular motion [6].

The b-value is a major determinant of the acquired diffusion signal and it is organ-dependent [14]. Low b-values (less than 200 s/mm²) yields higher SNR due to the cumulative effect of signal from perfusing vessels and the extracellular space. With increased b-values the perfusion inputs are eliminated and the extracellular space becomes the source of signal increasing lesion conspicuity [14,15].

Many b-values are required to deduct a quantitative metric; the ADC, that expresses the intra-voxel diffusion at different b-values. Using three b-values to calculate ADC is universally acceptable in different body regions, to keep the scan time within the scope of clinical utility and diagnostic value. Previous in-vivo trials found no significant difference in ADC values between 1.5 T and 3 T [16,17].

Many approaches have been used to overcome decreased SNR of DWI. These involved using short TE sequences, increasing interval between b-values, using reduced field of view (rFOV) and computed diffusion-weighted imaging (cDWI) techniques [18,19]. Further details on the principal and technical aspects of DWI are widely available in the literatures [6,14,15].

Beyond its original neuro-imaging applications, DW has been clinically exploited in oncologic and body imaging thanks to its simplicity, radiation-free nature, needless contrast administration, and convenience as well as outstanding sensitivity and specificity [6,20,21]. It has been clinically validated for screening of infiltrative primary and secondary osseous lesion as well as for assessing the response to chemotherapy using the whole body-diffusion weighted MR imaging (WB-DW MRI) [22,23]. However, fewer studies have deployed it to characterize exclusive osseous lesions with heterogeneous results [7,10,13,24–26].

Our study used the mean (mADC) value for its proven accuracy confirmed by previous literature [8–10,26]. We found that a mean ADC value of $\leq 1.1 \times 10^{-3}$ mm²/s was significantly able to discriminate between benign and malignant bone lesions at 3 T field strength, with high sensitivity; after exclusion of the debatable chondroid-rich neoplasms. This in agreement with previous published data [9,10,13,24–26].

Early infiltrative neoplastic bone marrow disease; by metastasis and blood dyscrasia, may overlap with benign focal marrow abnormalities e.g. reversion and hyperplasia. Therefore, follow-up exams and indeterminate nuclear scans may delay the diagnosis with dreadful consequences on patient's managements.

We empirically noticed higher ADC values of our incidentally detected bone lesions compared to the adjacent sampled areas of normal bone marrow. Albeit, we did not investigate this relationship as it had been exhaustively reported and settled in literature [9,27,28].

ADCs values of the normal adult marrow have been reported to be inherently low ($\sim 0.3\text{--}0.4 \times 10^{-3}$ mm²/sec) [27,28]. These had been related to the compound interplay of its buildup of: (i) tightly packed large fatty cells and interspersed red marrow elements in a scant extracellular matrix; providing scarce protons density, (ii) that are interwoven between the relatively thick bony trabeculae, with (iii) an overall low perfusion of the bone [27,28]. Contrarily, localized destruction of bony trabeculae, replacement of the normal bone marrow elements by neoplastic cells and extracellular matrix along with parasitic neo-angiogenesis and increased vascularity. These have been hypothesised to facilitate marrow diffusion and increase ADCs values in the abnormal bone marrow [27,28].

Overall, malignant bony neoplasms (both primary and secondary) exhibited lower ADC values as compared to the benign osseous lesions; in the current series, inferring diffusion restriction. This is comparable to previous clinical trials [7,9,10,13,24–26]. The main bulk of our malignant lesions included: Ewing's sarcoma, osteosarcoma, and primary lymphoma as well as bone metastases. This could be explained by the

fact that malignant tumors are characterized by increased number of compactly packed cells with high nuclear/ cytoplasmic ratio and paucity of extra-cellular matrix. Such tissue micro-environment would restrict the water diffusivity between the inter- and intra-cellular compartments [27,28]. Moreover, presence of ossifications in osteosarcoma would limit diffusivity [25].

In contrast to other malignant lesions in the current cohort; our three cases of chondrosarcoma returned high ADC readouts similar to those of benign lesions. This is in line with the studies of Douis et al. [8,29,30] who exploited the DW imaging in discerning benign and malignant cartilaginous lesions in both axial and appendicular skeletons. This is thought to be the result of the water-rich myxoid matrix of these tumors with sparse chondrocytes representing less available diffusion barriers [7].

In line with earlier studies [7,9,10,13,24–26], our benign neoplasms and neoplasm-like bony lesions recorded higher ADC values; reflecting less diffusion restriction. This might be attributed to their dominant tissue architecture that is usually composed of few cells imbedded in an abundant loose stroma [31]. This loose tissue architecture would mean less barriers to Brownian motion of water and facilitate tissue water diffusivity with subsequent higher ADC values. Paradoxically, the fibrous-rich lesions of this benign category recorded relatively contradictory ADC values. This could be explained by the notions of Wang et al. [25] who postulated that abundant collagen fibrillar networks and fibroblasts might conceivably limit free extracellular diffusion.

Our reasonable sensitivity and moderate specificity add to the previous published data and emphasises the potential capability of the ADC to give a global insight of tissue architectural build-up of an incidentally discovered osseous lesion. This might be caveated by the paradoxical readouts in the chondroid lesions. However, sound clinical practice recommends integrating the diffusion metrics with other conventional MR sequences, previous radiographic workup and clinical data to deduce a sound working diagnosis. This approach is projected to give a timely non-invasive prediction of biologic nature of such lesion; in-vivo, and obviates the need for more invasive procedures in the proper clinical scenario.

We acknowledge the following limitations of our study. Firstly, the retrospective nature of the study and our stringent inclusion and exclusion criteria may represent a selection bias. Nonetheless, as a tertiary musculoskeletal center we use dedicated protocols for proper patient selections via multidisciplinary team approach. Secondly, our sample size and lesions heterogeneity may affect the statistical results. However, this might be acceptable on the background of the known relatively low incidence of bone neoplasms and heterogeneity of their cells of origin [32]. Thirdly, our results are derived from a scanner of a single vendor with pre-set parameters and software that may not be applicable to others. Further comparative studies across different MRI platforms may be needed to address this issue. Another point is that just above a third of our cohort did not have a biopsy confirmation. However, in a real-world practice; the mere presence of a lesion does not necessitate histology confirmation thanks to the current accumulated clinical and imaging literature. These may sufficiently favor longitudinal non-invasive follow-up for non-aggressive lesions e.g. in case of enchondroma, or a new lesion in a patient with known primary malignancy [33]. Moreover, we did not include osseous benign lesions of non-neoplastic etiology e.g. bone abscess as the diagnosis of these lesions is usually straightforward by the clinical setting and other ancillary imaging features in a multidisciplinary clinical work environment.

In summary, our findings endorse the use of quantitative ADC as a non-invasive surrogate for discerning osseous lesions into benign or malignant, in-vivo. This might assuage the concerns of both patients and medical providers; alike and mitigate the need for further diagnostic workup and more invasive procedures.

Compliance with ethical standards

All subjects enrolled in the current study were treated following the national ethical standards and Helsinki declarations. This study was approved by our local institutional review board with patients' consent waiver due to the retrospective study design.

Funding

The authors declare that this research did not receive any specific grant from funding agencies in the public, commercial, or not-for-profit sectors.

Conflict of interest

The authors declare that; this research did not receive any specific grant from funding agencies in the public, commercial, or not-for-profit sectors.

References

- [1] S. Bernard, E. Walker, M. Raghavan, An approach to the evaluation of incidentally identified bone lesions encountered on imaging studies, *Am. J. Roentgenol.* 208 (2017) 960–970, <https://doi.org/10.2214/AJR.16.17434>.
- [2] L.M. Fayad, M.A. Jacobs, X. Wang, J.A. Carrino, D.A. Bluemke, Musculoskeletal tumors: how to use anatomic, functional, and metabolic MR techniques, *Radiology* 265 (2012) 340–356, <https://doi.org/10.1148/radiol.12111740>.
- [3] T. Liu, S. Wang, H. Liu, B. Meng, F. Zhou, F. He, X. Shi, H. Yang, Detection of vertebral metastases: a meta-analysis comparing MRI, CT, PET, BS and BS with SPECT, *J. Cancer Res. Clin. Oncol.* 143 (2017) 457–465, <https://doi.org/10.1007/s00432-016-2288-z>.
- [4] A.A. Malayeri, K.M. Brooks, L.H. Bryant, R. Evers, P. Kumar, D.S. Reich, D. A. Bluemke, National Institutes of Health perspective on reports of gadolinium deposition in the brain, *J. Am. Coll. Radiol. JACR* 13 (2016) 237–241, <https://doi.org/10.1016/j.jacr.2015.11.009>.
- [5] L.B. Mithal, P.S. Patel, D. Mithal, H.L. Palac, M.N. Rozenfeld, Use of gadolinium-based magnetic resonance imaging contrast agents and awareness of brain gadolinium deposition among pediatric providers in North America, *Pediatr. Radiol.* 47 (2017) 657–664, <https://doi.org/10.1007/s00247-017-3810-4>.
- [6] G.B. Chavhan, Z. Alsabban, P.S. Babyn, Diffusion-weighted imaging in pediatric body MR imaging: principles, technique, and emerging applications, *Radiogr. Rev. Publ. Radiol. Soc. N. Am. Inc.* 34 (2014) E73–E88, <https://doi.org/10.1148/rg.343135047>.
- [7] Y. Hayashida, T. Hirai, T. Yakushiji, K. Katahira, O. Shimomura, M. Imuta, T. Nakaura, D. Utsunomiya, K. Awai, Y. Yamashita, Evaluation of diffusion-weighted imaging for the differential diagnosis of poorly contrast-enhanced and T2-prolonged bone masses: initial experience, *J. Magn. Reson. Imaging JMRI* 23 (2006) 377–382, <https://doi.org/10.1002/jmri.20512>.
- [8] H. Douis, M.A. Davies, P. Sian, The role of diffusion-weighted MRI (DWI) in the differentiation of benign from malignant skeletal lesions of the pelvis, *Eur. J. Radiol.* 85 (2016) 2262–2268, <https://doi.org/10.1016/j.ejrad.2016.10.014>.
- [9] G. Pozzi, D. Albano, C. Messina, S.A. Angileri, A. Al-Mnayyis, F. Galbusera, A. Luzzati, G. Perrucchini, G. Scotto, A. Parafioriti, A. Zerbi, L.M. Sconfienza, Solid bone tumors of the spine: diagnostic performance of apparent diffusion coefficient measured using diffusion-weighted MRI using histology as a reference standard, *J. Magn. Reson. Imaging JMRI* (2017), <https://doi.org/10.1002/jmri.25826>.
- [10] S. Ahlawat, P. Khandheria, T.K. Subhawong, L.M. Fayad, Differentiation of benign and malignant skeletal lesions with quantitative diffusion weighted MRI at 3T, *Eur. J. Radiol.* 84 (2015) 1091–1097, <https://doi.org/10.1016/j.ejrad.2015.02.019>.
- [11] L.A. Espinosa, D.A. Jamadar, J.A. Jacobson, M.O. DeMaeseneer, F.S. Ebrahim, B. J. Sabb, M.T. Kretschmer, J.S. Biermann, S.-M. Kim, CT-guided biopsy of bone: a radiologist's perspective, *Am. J. Roentgenol.* 190 (2008) W283–W289, <https://doi.org/10.2214/AJR.07.3138>.
- [12] *Blinded*, (n.d.).
- [13] E. Oh, Y.C. Yoon, J.H. Kim, K. Kim, Multiparametric approach with diffusion-weighted imaging and dynamic contrast-enhanced MRI: a comparison study for differentiating between benign and malignant bone lesions in adults, *Clin. Radiol.* 72 (2017) 552–559, <https://doi.org/10.1016/j.crad.2017.02.017>.
- [14] T. Higaki, Y. Nakamura, F. Tatsugami, Y. Kaichi, M. Akagi, Y. Akiyama, Y. Baba, M. Iida, K. Awai, Introduction to the technical aspects of computed diffusion-weighted imaging for radiologists, *RadioGraphics* 38 (2018) 1131–1144, <https://doi.org/10.1148/rg.2018170115>.
- [15] T. Fukuda, K. Wengler, R. de Carvalho, P. Boonsri, M.E. Schweitzer, MRI biomarkers in osseous tumors: biomarkers in osseous tumors, *J. Magn. Reson. Imaging* 50 (2019) 702–718, <https://doi.org/10.1002/jmri.26672>.
- [16] H.J. Park, S.Y. Lee, M.H. Rho, E.C. Chung, M.S. Kim, H.J. Kwon, I.Y. Youn, Single-shot echo-planar diffusion-weighted MR imaging at 3T and 1.5T for differentiation of benign vertebral fracture edema and tumor infiltration, *Korean J. Radiol.* 17 (2016) 590–597, <https://doi.org/10.3348/kjr.2016.17.5.590>.
- [17] A.B. Rosenkrantz, M. Oei, J.S. Babb, B.E. Niver, B. Taouli, Diffusion-weighted imaging of the abdomen at 3.0 Tesla: image quality and apparent diffusion coefficient reproducibility compared with 1.5 Tesla, *J. Magn. Reson. Imaging JMRI* 33 (2011) 128–135, <https://doi.org/10.1002/jmri.22395>.
- [18] G. Zaharchuk, E.U. Saritas, J.B. Andre, C.T. Chin, J. Rosenberg, T.J. Brosnan, A. Shankaranarayanan, D.G. Nishimura, N.J. Fischbein, Reduced field-of-view diffusion imaging of the human spinal cord: comparison with conventional single-shot echo-planar imaging, *AJNR Am. J. Neuroradiol.* 32 (2011) 813–820, <https://doi.org/10.3174/ajnr.A2418>.
- [19] S. Gatidis, H. Schmidt, P. Martirosian, K. Nikolaou, N.F. Schwenzer, Apparent diffusion coefficient-dependent voxelwise computed diffusion-weighted imaging: an approach for improving SNR and reducing T2 shine-through effects, *J. Magn. Reson. Imaging JMRI* 43 (2016) 824–832, <https://doi.org/10.1002/jmri.25044>.
- [20] A.R. Padhani, Diffusion magnetic resonance imaging in cancer patient management, *Semin. Radiat. Oncol.* 21 (2011) 119–140, <https://doi.org/10.1016/j.semradonc.2010.10.004>.
- [21] O. Freihat, T. Pinter, A. Kedves, D. Sipos, Z. Cselik, I. Repa, Á. Kovács, Diffusion-weighted imaging (DWI) derived from PET/MRI for lymph node assessment in patients with Head and Neck Squamous Cell Carcinoma (HNSCC), *Cancer Imaging Off. Publ. Int. Cancer Imaging Soc.* 20 (2020) 56, <https://doi.org/10.1186/s40644-020-00334-x>.
- [22] A.S. Littooji, T.C. Kwee, B. de Keizer, M.C.A. Bruin, A. Coma, F.J.A. Beek, R. Fijnheer, R.A.J. Nievelstein, Whole-body MRI-DWI for assessment of residual disease after completion of therapy in lymphoma: a prospective multicenter study, *J. Magn. Reson. Imaging JMRI* 42 (2015) 1646–1655, <https://doi.org/10.1002/jmri.24938>.
- [23] C. Lacognata, F. Crimi, A. Guolo, C. Varin, E. De March, S. Vio, A. Ponzoni, G. Barilà, A. Lico, A. Branca, E. De Biasi, F. Gherlinzoni, V. Scapin, E. Bissoli, T. Berno, R. Zambello, Diffusion-weighted whole-body MRI for evaluation of early response in multiple myeloma, *Clin. Radiol.* 72 (2017) 850–857, <https://doi.org/10.1016/j.crad.2017.05.004>.
- [24] Y. Pekcevik, M.O. Kahya, A. Kaya, Diffusion-weighted magnetic resonance imaging in the diagnosis of bone tumors: preliminary results, *J. Clin. Imaging Sci.* 3 (2013) 63, <https://doi.org/10.4103/2156-7514.124094>.
- [25] T. Wang, X. Wu, Y. Cui, C. Chu, G. Ren, W. Li, Role of apparent diffusion coefficients with diffusion-weighted magnetic resonance imaging in differentiating between benign and malignant bone tumor, *World J. Surg. Oncol.* 12 (2014), <https://doi.org/10.1186/1477-7819-12-365>.
- [26] J. Cao, L. Xiao, B. He, G. Zhang, J. Dong, Y. Wu, H. Xie, G. Wang, X. Lin, Diagnostic value of combined diffusion-weighted imaging with dynamic contrast enhancement MRI in differentiating malignant from benign bone lesions, *793.e1-793.e9, Clin. Radiol.* 72 (2017), <https://doi.org/10.1016/j.crad.2017.04.017>.
- [27] C. Messiou, D.J. Collins, V.A. Morgan, N.M. Desouza, Optimising diffusion weighted MRI for imaging metastatic and myeloma bone disease and assessing reproducibility, *Eur. Radiol.* 21 (2011) 1713–1718, <https://doi.org/10.1007/s00330-011-2116-4>.
- [28] A.R. Padhani, K. van Ree, D.J. Collins, S. D'Sa, A. Makris, Assessing the relation between bone marrow signal intensity and apparent diffusion coefficient in diffusion-weighted MRI, *AJR Am. J. Roentgenol.* 200 (2013) 163–170, <https://doi.org/10.2214/AJR.11.8185>.
- [29] H. Douis, L. Jeys, R. Grimer, S. Vaipuri, A.M. Davies, Is there a role for diffusion-weighted MRI (DWI) in the diagnosis of central cartilage tumors? *Skelet. Radiol.* 44 (2015) 963–969, <https://doi.org/10.1007/s00256-015-2123-7>.
- [30] H. Douis, L. Singh, A. Saifuddin, MRI differentiation of low-grade from high-grade appendicular chondrosarcoma, *Eur. Radiol.* 24 (2014) 232–240, <https://doi.org/10.1007/s00330-013-3003-y>.
- [31] E.F. McCarthy, CT-guided needle biopsies of bone and soft tissue tumors: a pathologist's perspective, *Skelet. Radiol.* 36 (2007) 181–182, <https://doi.org/10.1007/s00256-006-0244-8>.
- [32] A. Franchi, Epidemiology and classification of bone tumors, *Clin. Cases Miner. Bone Metab. Off. J. Ital. Soc. Osteoporos. Miner. Metab. Skelet. Dis.* 9 (2012) 92–95.
- [33] C.G. Cronin, T. Cashell, J.N. Muirheartaigh, R. Swords, M. Murray, G. J. O'Sullivan, D. O'Keefe, Bone biopsy of new suspicious bone lesions in patients with primary carcinoma: prevalence and probability of an alternative diagnosis, *AJR Am. J. Roentgenol.* 193 (2009) W407–W410, <https://doi.org/10.2214/AJR.08.1882>.